Study of the Coupling Between Human Head and Cellular Phone Helical Antennas

Stavros Koulouridis and Konstantina S. Nikita, *Senior Member, IEEE*

***Abstract*—The interaction between normal-mode helical antennas and human head models is analyzed, using both a novel accurate semi-analytical method and finite-difference time-domain (FDTD) simulations. The semi-analytical method is based on the combination of Green's functions theory with the method of moments (Green/MoM) and is able to model arbitrarily shaped wire antennas radiating in the close proximity of layered lossy dielectric spheres representing simplified models of the human head. The purpose of the development of the Green/MoM technique is to provide a reliable tool for preliminary (worst case) estimation of human head exposure to the field generated by different antenna configurations with emphasis on the helical antenna, representing the most diffused antenna type used in modern cellular handsets. Furthermore, the accurate semi-analytical character of the Green/MoM technique permits the accuracy assessment of purely numerical techniques, such as the FDTD, which is currently the most widely used computational method in mobile communication dosimetric problems, since it allows modeling of anatomically based head models. After appropriate benchmarking, FDTD simulations are used to study the interaction between a heterogeneous anatomically correct model of the human head exposed to a normal-mode helix monopole operating at 1710 MHz mounted on the top of a metal box representing a realistic mobile communication terminal. The study of both canonical and realistic exposure problems includes computations of specific absorption rates (SARs) inside the human head, total power absorbed by the head and assessment of antenna performance. Emphasis is placed on the comparative dosimetric assessment between adults and children head models.**

***Index Terms*—Biological effects of electromagnetic radiation, helical antenna, human head of adults and children, mobile phone, semi-analytical and finite-difference time-domain (FDTD) techniques.**

I. Introduction

THE wide expansion of cellular phones around the world is indisputable. The phone radiating element used to vary, in previous years, among quarter-wavelength, half-wavelength, three quarter-wavelength linear antennas and whip antennas. These antenna models have been extensively used to equip various cellular handsets. In the last few years, however, different antenna designs have been proposed, motivated by the need to reduce the size of handset devices while keeping radiation characteristics similar with the "older" antenna models. One of the most diffused new antenna types is the helical antenna. Helical antennas have been used in the last 40 years and, in general, radiate in two modes depending on their dimensional characteristics [1]. For mobile communication handsets, helical antennas are constructed to radiate in normal mode, hence their physical dimensions are very small compared to the radiation wavelength.

The evaluation of the power absorbed by the user's head as well as the antenna performance in the presence of the user's head represent key tasks for both design and compliance testing of cellular phones. These tasks can be efficiently addressed by means of numerical techniques, with the finite-difference time-domain (FDTD) method [2], [3] dominating over the other numerical methods in recent years, due to its simplicity and its ability to treat highly nonhomogeneous structures. Although FDTD is able to model anatomically detailed human head structures, significant difficulties are encountered in modeling antenna structures not conforming to the used grid. Thus, while monopole and planar antennas can be easily implemented within FDTD codes, modeling of a helix can become a rather difficult task. In fact, rather large structures have been analyzed using a pure FDTD scheme [4], [5], while for smaller structures a graded mesh [6], equivalent sources [7], [8], and a hybrid method of moments (MoM) /FDTD [9], [10] have been proposed. Furthermore, even if intensive research work with the FDTD method has led to high confidence in the obtained results, the exact error estimation of FDTD simulations still remains a difficult task. It has been shown that uncertainties are involved and discrepancies can be observed in the results obtained by different research groups nominally using the same numerical method, even for well defined canonical cases involving linear dipoles [11].

Due to the above described problems in FDTD modeling of the helical antenna and uncertainties encountered in FDTD modeling even for linear antenna structures, the availability of accurate methods able to treat canonical exposure problems becomes of primary importance. Such methods can provide an efficient tool for benchmarking of purely numerical techniques (FDTD), which can then be used to analyze realistic exposure problems.

In this paper, the electromagnetic dosimetry problem referring to the exposure of human head models to helical antennas is treated in detail. To this end, a semi-analytical technique is proposed, based on the use of the dyadic Green's function theory [12], [13] and the MoM (Green/MoM), for studying the interaction between a layered spherical head model and an arbitrarily shaped wire antenna. The proposed method provides a means of (worst case) preliminary estimation of the human head exposure to the field generated by different wire antenna configurations such as helical or linear dipoles. It is also employed as a reliable

Manuscript received October 31, 2002; revised June 14, 2003. The work of S. Koulouridis was supported by the Hellenic State Scholarships Foundation.

The authors are with the National Technical University of Athens, School of Electrical and Computer Engineering, 15780 Athens, Greece (e-mail: knikita@cc.ece.ntua.gr).

Digital Object Identifier 10.1109/TEMC.2004.823612

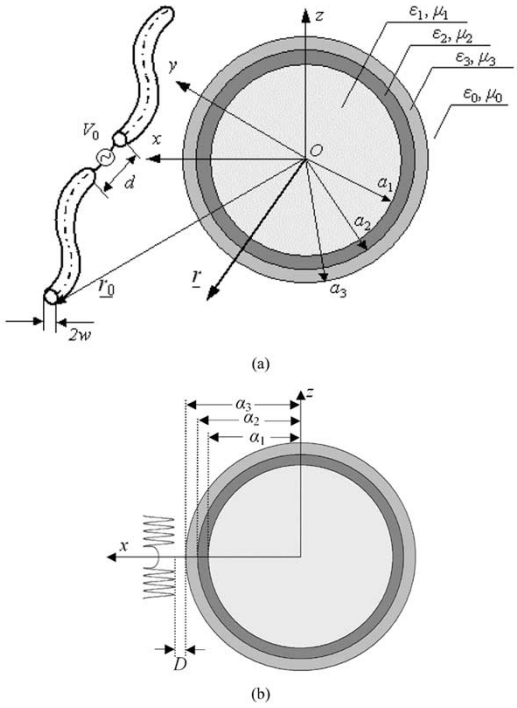

Fig. 1. Schematic diagram of a three-layer spherical head model exposed to the radiation of: (a) arbitrarily shaped wire antenna and (b) helical antenna (not drawn in scale).

tool for checking the accuracy of FDTD simulations which are then used to solve the electromagnetic dosimetry problem for a heterogeneous anatomically correct human head model exposed to a handheld terminal equipped with a normal-mode helical antenna. Furthermore, in this paper emphasis is placed on the comparative study of power absorption between heads of adults and children, and extensive simulations based on both Green/MoM and FDTD techniques are carried out.

The rest of the paper is organized as follows. In Section II, the mathematical formulation of the hybrid Green/MoM technique is presented, while in Section III, details of FDTD simulations for the cases studied in this paper are given. In Section IV, the head and antenna models used in the simulations are described. In Section V, the necessary checks for the validation of the Green/MoM technique are presented, followed by numerical results concerning the absorption by the head and the antenna performance for specific canonical exposure problems, i.e., layered spheres and helical dipoles at 1710 MHz based on Green/MoM and FDTD simulations. Finally, results of FDTD simulations for a realistic exposure problem, i.e., an MRI-based human head model exposed to a handset equipped with a small helix-monopole operating at 1710 MHz, are presented.

II. Green/MoM Technique: Mathematical Formulation and Analysis

The problem under consideration is shown in Fig. 1. A three-layer sphere with radii α_1, α_2, and α_3 is used to model the head. The relative complex permittivity of each layer is $\varepsilon_1, \varepsilon_2$, and ε_3, respectively. The magnetic properties of the layers are defined as $\mu_1 = \mu_2 = \mu_3 = \mu_0$. Free space is assumed for the exterior of the sphere with wavenumber $k_0 = \omega\sqrt{\varepsilon_0\mu_0}$, where ω is the radian frequency, ε_0 and μ_0 are the free-space permittivity and permeability, respectively. A perfectly conducting arbitrarily shaped wire excited by a voltage imposed at a feeding gap of length d models the antenna. The time dependence of the field quantities is assumed to be $e^{-j\omega t}$ and it is suppressed throughout the following analysis.

First, the Green's function of the three-layer sphere is determined as the response of this object to the excitation generated by an elementary dipole of unit dipole moment, external to the sphere. Thus, the following expression for the electric type Green's function inside the layered sphere $(i = 1, 2, 3)$ and in the air region $(i = 4)$ is obtained [14]:

$$\begin{aligned}\overline{G}_i(\underline{r},\underline{r}') = \sum_{n=1}^{+\infty}\sum_{m=-n}^{n} \frac{jk_0(-1)^m(2n+1)}{4\pi n(n+1)} \\ \times\Big\{\Big[Q_n^{(i,1)}\underline{m}_{mn}^{(1)}(\underline{r},k_i) + Q_n^{(i,2)}\underline{m}_{mn}^{(j)}(\underline{r},k_i)\Big] \\ \times \underline{m}_{-mn}^{(3)}(\underline{r}',k_0) \\ + \Big[R_n^{(i,1)}\underline{n}_{mn}^{(1)}((\underline{r},k_i)) + R_n^{(i,2)}\underline{n}_{mn}^{(j)}(\underline{r},k_i)\Big] \\ \times \underline{n}_{mn}^{(3)}(\underline{r}',k_0)\Big\} \end{aligned} \quad (1)$$

where $\underline{m}$ and $\underline{n}$ are the well-known spherical wave vectors [12], Q, R are scalar coefficients computed in [14] and $k_i = \omega\sqrt{\varepsilon_i\mu_i}$, $i = 1, 2, 3$ is the wavenumber in the ith region. Also $\ell = 2$ for $i = 1, 2, 3$ and $\ell = 3$ for $i = 4$.

The antenna of the problem under consideration is modeled by applying the MoM. The geometry of an arbitrarily shaped wire antenna, in the global Cartesian coordinates system Oxyz (Fig. 1), is parametrically described as [15],

$$\underline{r}(t) = \underline{r}_0 + x(t)\hat{x} + y(t)\hat{y} + z(t)\hat{z} \quad (2)$$

where t is a real valued parameter.

For the problem of the wire antenna treated in this paper, since its diameter is usually substantially less than the radiation wavelength, the thin wire approximation (TWA) can be adopted [16]. Thus, the current on the surface of the antenna wire is supposed to flow parallel to its curved axis. The antenna is then subdivided into a number of J curved segments, Δt in length, centered at points $t_j = (j-1)\Delta t + \Delta t/2$, $j = 1, \ldots, J$. The electric field at a point $\underline{r}$ lying in any region $(i = 1, 2, 3, 4)$, is expressed by means of the corresponding Green's function

$$\underline{E}_i(\underline{r}) = j\omega\mu_0 \sum_{j=1}^{J} \int_{t_j-\Delta t/2}^{t_j+\Delta t/2} \overline{G}_i(\underline{r},\underline{r}')\hat{s}(t')I_j(\underline{r}')dt' \quad (3)$$

where I_j is the unknown current coefficient flowing along the curved jth segment of the antenna wire and $\hat{s}$ is the unit vector tangent to the wire antenna,

$$\hat{s}(t) = \frac{\frac{d\underline{r}}{dt}}{\sqrt{\left|\frac{d\underline{r}}{dt}\right|^2}}. \quad (4)$$

Then, the boundary conditions for the tangential electric field component vanishing on the conducting surface of the

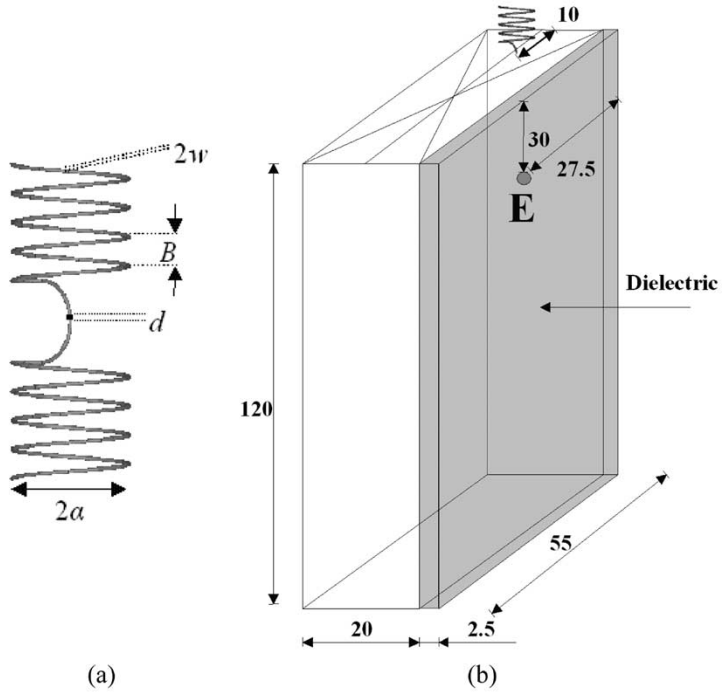

Fig. 2. (a) Normal-mode helical dipole antenna. (b) Handset equipped with a helix monopole. Dimensions in millimeters. Point E corresponds to the projection of the ear canal.

antenna—with the exception of the feeding gap—are imposed at J points lying along a line on the surface of the antenna wire

$$\hat{s}(t_k)\cdot\underline{E}_4(\underline{r}_k) = \begin{cases} 0, & \text{if } \underline{r}_k \text{ lies on the metallic surface} \\ \frac{V_0}{d}, & \text{if } \underline{r}_k \text{ lies in the feeding gap} \end{cases} \quad (5)$$

where $\underline{E}_4$ is computed by (3) for $i = 4$ and $k = 1, \ldots, J$. The length d of the feeding gap is assumed to be sufficiently small compared to the wire radius, so that the electric field inside the feeding gap can be considered constant. The points $\underline{r}_k$ are given as

$$\underline{r}_k = \underline{r}_0 + x(t_k)\hat{x} + y(t_k)\hat{y} + z(t_k)\hat{z} + w\hat{n}(t_k) \quad (6)$$

where w is the radius of the wire, $\hat{n}$ is the unit normal vector, $k = 1, \ldots, J$

$$\hat{n}(t) = \frac{\frac{d^2\underline{r}}{dt^2}}{\sqrt{\left|\frac{d^2\underline{r}}{dt^2}\right|^2}}. \quad (7)$$

By enforcing (5), a $J \times J$ system of linear equations is obtained, which is solved for the unknown current coefficients I_j. Once these coefficients are computed, the electric field at any point inside and outside the spherical head model can be calculated, by using the closed-form equation (3).

For the specific case of a helical antenna with helix radius α, and pitch B (Fig. 2(a)), (2) takes the form

$$\underline{r} = \underline{r}_0 - (a\ \cos\ t)\hat{x} + (a\ \sin\ t)\hat{y} + \frac{Bt}{2\pi}\hat{z} \quad (8)$$

while the unit tangential and normal vectors are given as

$$\hat{s}(t) = \frac{1}{\sqrt{a^2 + \left[\frac{B^2}{(4\pi^2)}\right]}} \times \left(-(a\ \sin\ t)\hat{x} + (a\ \cos\ t)\hat{y} + \frac{B}{2\pi}\hat{z}\right) \quad (9)$$

$$\hat{n}(t) = \frac{1}{\sqrt{a^2 + \left[\frac{B^2}{(4\pi^2)}\right]}}\left(-(\cos\ t)\hat{x} - (\sin\ t)\hat{y}\right). \quad (10)$$

Once the electric field inside the spherical head model is computed, then, the specific absorption rate (SAR) at any point inside the head tissues can be calculated as

$$SAR(\underline{r}) = \frac{\sigma(r)|\underline{E}_i(\underline{r})|^2}{\rho(\underline{r})} \quad (11)$$

where σ (Si/m), ρ (kg/m^3) represent the specific conductivity and the mass density, respectively, of the tissue at the point of interest, $|\underline{E}_i(\underline{r})|$ is the magnitude of the electric field at the same point and $i = 1, 2, 3$. Calculation of SAR averaged over a reference mass M (1 gr or 10 gr) of tissue, as required by the safety guidelines [17]–[21], is carried out using

$$SAR_M(\underline{r}) = \frac{\iiint_{V=\delta^3} SAR(\underline{r}')\rho(\underline{r}')d\underline{r}'}{\iiint_{V=\delta^3} \rho(\underline{r}')d\underline{r}'} \quad (12)$$

where the denominator represents the mass contained in a cubic cell of volume δ^3 centered at point $\underline{r}$, which should be equal to the reference mass M. In general, for the case of a layered sphere, the size of the cube centered at the point of interest containing the reference mass M is not *a priori* known and has to be

determined, by applying an iterative procedure. In the present study the averaging procedure has been performed for a cube full of tissue. The power absorbed by the head is computed as

$$P_{abs} = \int_{\theta=0}^{\pi} \int_{\varphi=0}^{2\pi} \int_{r=0}^{a_3} \sigma(\underline{r}) |\underline{E}(\underline{r})|^2 r^2 \sin\theta \, dr \, d\varphi \, d\theta. \quad (13)$$

III. FDTD Simulations

Simulations using XFDTD, a commercially available software package have also been carried out [22]. A rectangular computational grid, based on the Yee cell, with a resolution of 1.25 mm and the total-field formulation have been used, while the perfectly matched layer (PML) absorbing boundary conditions with 8 PMLs have been employed [23]. The boundaries were placed 30 cells away from the nearest scatterer. Converged results have been assured by using 12 time periods. The helix geometry has been approximated in the FDTD grid as a rectangular helix of wires using perfect conducting cell edges. The excitation has been modeled by imposing a harmonic voltage at a vertical one-cell feeding gap. The current flowing through the voltage source cell has been calculated by integrating the magnetic fields around the voltage source according to Ampere's law. The input impedance of the antenna has then been derived from the ratio of the voltage and the current together with their phase difference. The accuracy of FDTD simulations has been checked against results produced by the Green/MoM technique for canonical problems.

Averaged SARs over a reference mass M (1 or 10 g) are calculated by an interpolation scheme. Cubical spaces centered on a cell are formed and the mass and average SAR of the sample cubes are found. The size of the sample cube increases until the total enclosed mass exceeds the reference mass M. The sample cube increases in odd-numbered steps ($1 \times 1 \times 1$, $3 \times 3 \times 3$, $5 \times 5 \times 5$ etc) to remain centered on the desired cell. The sample cube must meet some conditions to be considered valid. The cube may contain some nontissue cells, but it cannot contain an entire side or corner of nontissue cells. If the cube is found to be invalid, the averaging for the center cell stops and the same procedure is performed for the next center cell.

IV. Head and Antenna Models

Two spherical adult head models have been considered, namely, a homogeneous one consisting of brain tissue, and a three-layer one consisting of skin, skull and brain tissues. Both head models have a diameter of $2a_3 = 20$ cm, while the thicknesses of the skin and skull layers for the layered head model are assumed to be $a_3 - a_2 = 0.5$ cm and $a_2 - a_1 = 0.5$ cm, respectively. Table I summarizes the mass density (ρ), the dielectric constant (ε_r), and the conductivity (σ) of the tissues used for the calculations at 1710 MHz [24].

Apart from canonical head models, a realistic adult head model developed from magnetic resource imaging (MRI) scans of a human head has also been studied. The head model has been provided by Bradford University [25], has a spatial resolution of 1.25 mm and consists of 13 different tissues/organs.

TABLE I
Real Part (ε_r) of Dielectric Permittivity, Conductivity (σ), and Mass Density (ρ) of Tissues Used in Simulations for Canoncial Exposure Problems at 1710 MHz

Tissue	ε_r	σ (S/m)	ρ (kg/m^3)
Skin	38.2	0.941	1100
Bone (cortical/skull)	12.0	0.285	1200
Brain (grey matter)	51.8	1.521	1050

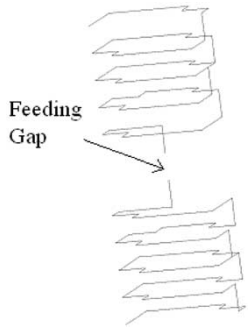

Fig. 3. FDTD model of the helical dipole with horizontal sections consisting of four cells and one cell vertical step.

Electrical characterization of the head tissues has been based on literature data [24].

In order to assess differences in energy absorption between adults and children, different sizes of head models have been considered. The children head models have been obtained from the adults ones by considering that the height of an average male adult is 176 cm while its weight is 71 kg. In the dosimetry handbook [26], the height and weight for an average 10-year old child are given as 138 cm and 32.5 kg respectively. Therefore all dimensions in both canonical and realistic adult head models have been changed by a factor of $((176/138) \cdot (32.5/71))^{1/2}$. The realistic child head model has been produced from the adult one by first changing the spatial resolution of the adult head model by the above mentioned factor and then by resampling the altered head model into 1.25 mm grid size.

Simulations for a normal-mode helical dipole operating at 1710 MHz have been carried out. The dipole antenna consists of a right-handed helix connected in series with a left handed helix, being the mirror image of the former with respect to the $z = 0$ plane [Fig. 2(a)] [9]. A circular arc is used to provide smooth transition of each helix to the axial feeding. The geometrical details of the examined helical antenna [Fig. 2(a)] are: $a = 2.5$ mm, $B = 1.25$ mm, $w = 0.1$ mm, $L = 4 + 4$ turns, $d = 0.2$ mm. The helix antenna model has been constructed in the FDTD grid as a rectangular helix of wires with horizontal sections consisting of four cells and a vertical step of one cell (Fig. 3). Furthermore, the above described right handed helix ($L = 4$ turns) monopole, mounted on the top corner of a metal handset box [Fig. 2(b)] has been studied. The dimensions of the metal box are $12 \times 5.5 \times 2$ cm^3 and its front face is covered with a low loss dielectric $(\varepsilon_r = 2.7 - j0.016)$, with a thickness of 2.5 mm. Point E in Fig. 2(b) corresponds to the projection of the ear canal to the dielectric front face of the handset.

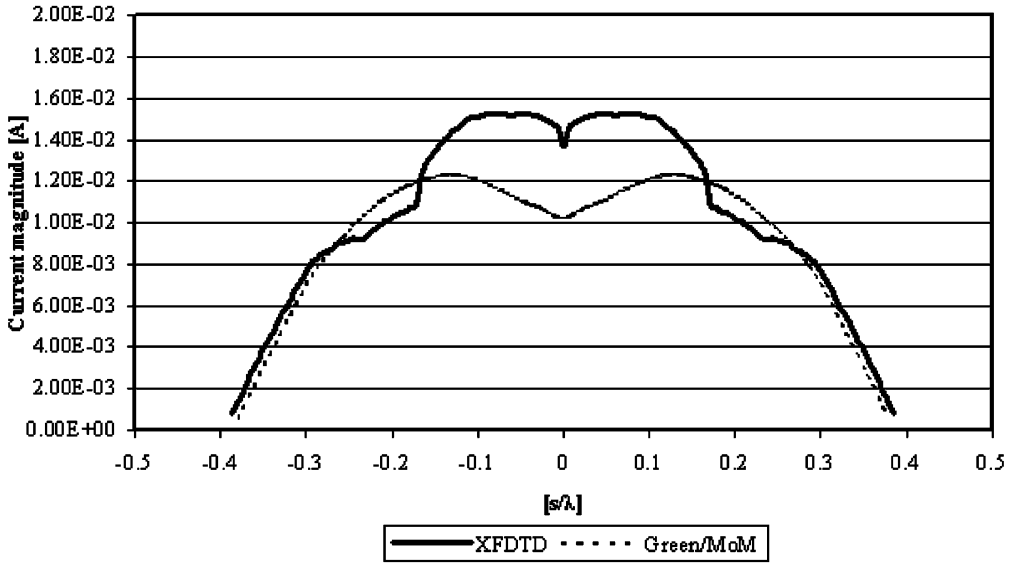

Fig. 4. Current distributions along the helical dipole radiating in the proximity of a homogeneous head model for a feeding voltage of 1 V. Results produced with Green/MoM and FDTD techniques.

V. Numerical Results and Discussion

A. Validation of the Green/MoM Technique

In order to check the convergence and stability of the developed Green/MoM numerical code, several trials have been performed by varying the number of spherical wave vectors used to express the fields inside the sphere layers and in the air region and by increasing the number of segments of the antenna wire. To assure convergence of the obtained solution at any point in space, a number of 35–65 wave vectors ((1)) is required, while a significantly lower number ($\sim$10) of wave vectors is needed for computations at far-field points. The number of segments required to model the wire antenna depends on its total length and complexity of its shape. For the specific helical dipole simulations considered here, a number of 500 segments has been found sufficient to assure convergence of the obtained solution.

An additional check referring to the energy conservation has been performed by comparing the input power computed at the feeding gap, to the sum of the power absorbed by the head and the power radiated in the antenna far field. An excellent agreement has been observed (difference less than 1%).

B. SAR Computations and Antenna Performance

The Green/MoM technique has been used to study canonical exposure problems at 1710 MHz. Simulations have been carried out for four spherical head models, namely homogeneous and three-layer spheres simulating adults and children heads, exposed to the helical dipole of Fig. 2(a). A separation distance of $D = 5$ mm between helical antenna and spherical head models has been considered.

For the case of the helical dipole radiating in the presence of the adult homogeneous spherical head model, the spatial distribution of the current along the antenna wire as a function of s/λ ratio, where s is the curvilinear coordinate along the wire, has been calculated and is presented in Fig. 4, for a feeding voltage of 1 V. The corresponding input impedance was found $5.1 + j85.68\ \Omega$.

TABLE II
Peak SAR Values and Absorbed Power in Homogeneous and Three-Layer Spherical Head Models Exposed to Normal–Mode Helical Dipole Antenna at 1710 MHz. The Total Radiated Power is 125 mW. Results Produced With Green/MoM and FDTD (†) Techniques

		Local SAR_{max} (W/kg)	1g-SAR_{max} (W/kg)	10g-SAR_{max} (W/kg)	Absorbed Power (mW)
Homogeneous	Adult	24.73 (25.32†)	14.39 (13.80†)	5.38 (6.01†)	114.84 (114.94†)
	Child	24.31 (25.34†)	13.98 (14.02†)	5.49 (6.09†)	112.75 (113.54†)
Three-layer	Adult	14.09 (15.17†)	6.97 (6.42†)	3.42 (3.83†)	117.27 (116.95†)
	Child	13.88 (15.51†)	7.70 (7.21†)	4.41 (4.82†)	119.01 (117.63†)

The maximum values of local SAR, SAR averaged over 1 or 10 g of tissue, and the power absorbed by the head have been computed for the four canonical problems and are shown in Table II. It can be noticed that similar values of maximum SAR (local or averaged) are observed in children and adults head models. As far as the total absorbed power is considered, a 90%–95% of the helical dipole input power is absorbed by children or adults head models.

Penetration curves showing the SAR variation along x-axis, that is "from one ear to the other" of the spherical head models, have also been computed and the local SAR values normalized to the maximum SAR value, as computed by the Green/MoM technique, are presented in Fig. 5. Since the diameter of the children's head models is smaller, the SAR value at the opposite from the phone head side is higher than the corresponding one in the adults head models.

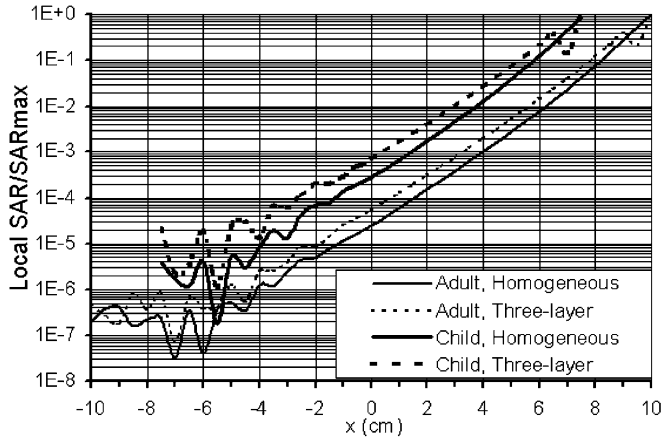

Fig. 5. Local SAR/$\mathrm{SAR}_{\max}$ distribution along x axis induced in adults' and children' spherical head models by the helical dipole. Computations using the Green/MoM technique.

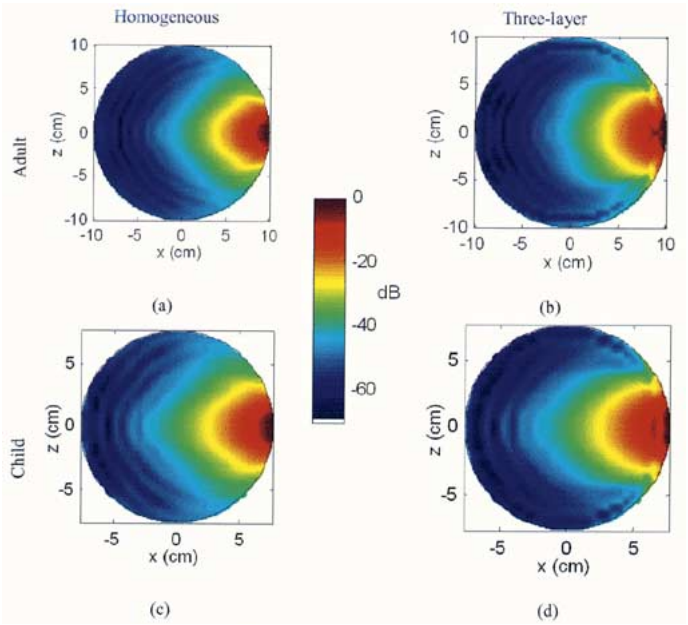

Fig. 6. Local SAR/$\mathrm{SAR}_{\max}$ distribution in decibels on the $y = 0$ plane for (a), (b) adults, and (c),(d) children head models exposed to the radiation of a helical dipole antenna at 1710 MHz. (a) and (c) homogeneous head models; (b) and (d) three-layer head models. Computations with the Green/MoM technique.

The distributions of the local SAR, at the $y = 0$ plane are shown in Fig. 6. It can be easily observed that high SAR regions in the children head models are more extended as compared to those in the adults head models, since the helical dipole physical dimensions relative to children head models dimensions are larger.

The influence of the head models on the radiation characteristics of the helical dipole has also been studied. Far field radiation patterns for the helical dipole in the presence of the homogeneous or the layered spherical head models have been calculated for the xy ($\theta = 90°$) and the xz ($\varphi = 0°$) planes and are shown in Fig. 7. The far-field radiation pattern in the direction of the head is significantly disturbed since the power is

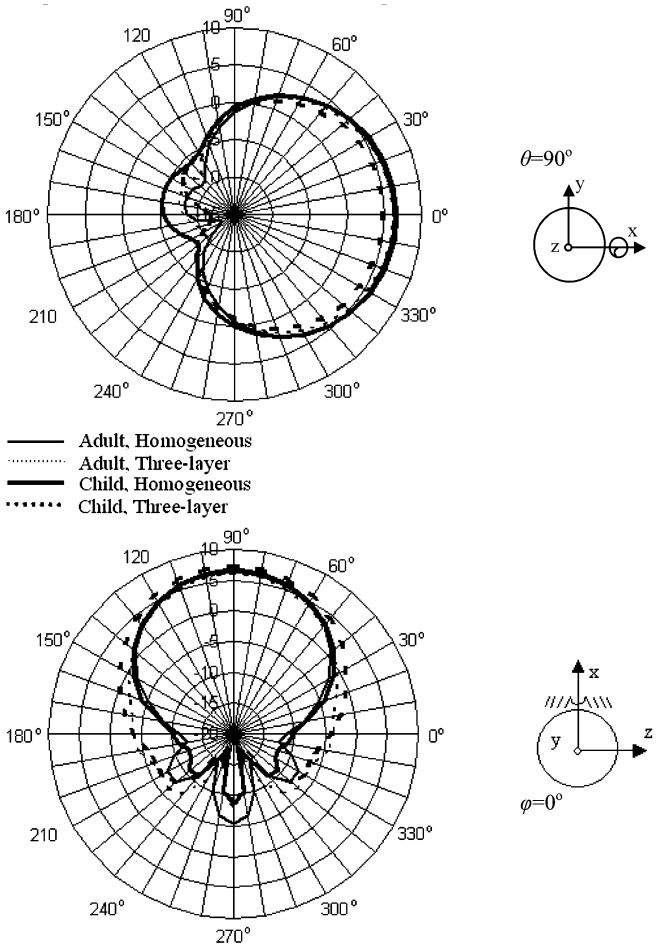

Fig. 7. Radiation pattern (decibels relative to isotropic radiator) for a helical dipole radiating in the presence of adults and children, homogeneous or three-layer spherical head models at 1710 MHz. Computations with the Green/MoM technique.

TABLE III
PEAK SAR VALUES AND ABSORBED POWER IN REALISTIC ADULT AND CHILD HEAD MODELS EXPOSED TO A HANDSET EQUIPPED WITH A HELIX MONOPOLE AT 1710 MHZ. THE TOTAL RADIATED POWER IS 125 mW

	Local SAR_{max} (W/kg)	1g-SAR_{max} (W/kg)	10g-SAR_{max} (W/kg)	Absorbed Power (mW)
Adult	5.70	2.42	1.35	82.81
Child	5.14	2.20	1.45	82.45

strongly absorbed by the head. The slight asymmetry observed on the xz plane can be explained by the asymmetry of the curved segments providing connection to the axial feeding gap of the dipole.

The above presented canonical exposure problems have also been studied using the XFDTD code. The spatial distribution of the current along the antenna wire as computed by the FDTD, for the case of the helical dipole radiating in the presence of

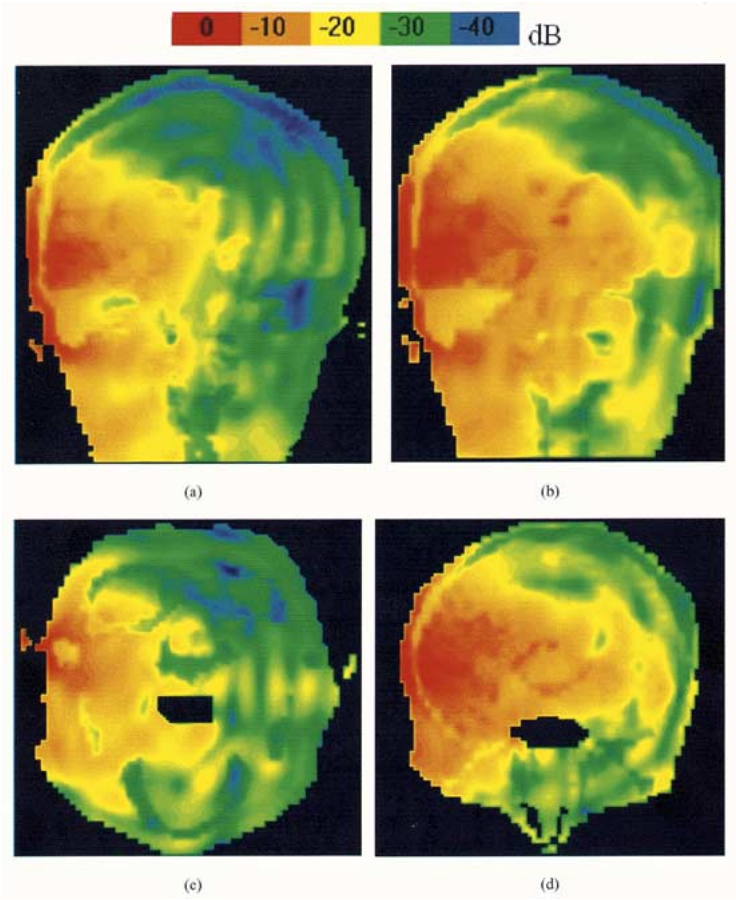

Fig. 8. Local SAR/$\mathrm{SAR}_{\max}$ distribution in decibels (a), (c) adult, and (b), (d) child. Head models in the proximity of a handset equipped with a helical monopole antenna at 1710 MHz on the (a), (b) xz, and (c), (d) xy slices where maximum local SAR is calculated. Handset in direct contact with ear.

the adult homogeneous head model is presented in Fig. 4, along with Green/MoM predictions, for comparative purposes. The FDTD calculated input impedance was $5.48 + j72.93\,\Omega$, which is in close agreement with the corresponding value predicted by the Green/MoM technique. The differences observed in the current distribution can be explained by the rectangular discretization of the helix wire and the wire parts providing connection to the axial feeding gap, in the FDTD grid.

The results for SAR and absorbed power values obtained by using the FDTD for the studied canonical exposure problems are shown in Table II against those obtained by the Green/MoM technique. The difference in the predicted values of maximum local SAR ranges from 2% to 12%, with the larger difference corresponding to the layered head models. The difference in averaged SAR values ranges from 0.5 to 8% for $M = 1$ g and is of the order of 10% for $M = 10$ g. The rather larger differences observed in the case of averaging over 10-g of tissue are related to differences in building the 10-g cube, between the two methods as described in Sections II and III, and especially in building the 10 g-cube surface close to the external head surface. Moreover, as far as the power absorbed by the user's head is considered, the discrepancy between Green/MoM and FDTD predictions is of the order of 1%.

Next, XFDTD simulations have been used to study the coupling between realistic MRI-based head models of an adult and a 10-year-old child exposed to the handset shown in Fig. 2(b). The handset is placed on a vertical position in direct contact with the ear. Point E [Fig. 2(b)] is placed at the ear canal. Results for maximum local SAR, averaged SAR and power absorption are presented in Table III. It can be noticed that although the local SAR value observed in the child's head is lower than the corresponding one in the adult's head, a slightly higher value of SAR averaged over 10 g is observed in the child's head. For direct contact of the handset to the head models, almost 65% of the antenna input power is absorbed by the child's or the adult's head. SAR distributions are presented in Fig. 8 for the slices where maximum SAR value has been calculated. SAR distribution is strongly inhomogeneous. High SAR regions in the child's head model are more extended as compared to those in the adult's head.

All the results presented in Tables II and III refer to a total radiated power of 125 mW. The total power radiated from the source, calculated at the feeding gap, has been imposed by using the equation $P_i = Re\{V \cdot I^*\}$, where V and I denote the voltage and the current at the center of the feeding gap and $*$ denotes the complex conjugate.

It is important to note that higher maximum SAR values are produced by the helical antenna as compared with published results for linear antennas [5], [27], due to the greater field concentration by the physically shorter helical antenna. For the same reason, rather high power absorption by the head models and consequently low radiation efficiency is observed, as computed by both Green/MoM and FDTD methods. Similar values for the absorbed power (80%) are reported in [6] for a dual-band monopole-helix antenna phone radiating in the close proximity of a realistic head model, at the frequency of helix antenna operation.

VI. Conclusion

The interaction between helical type antennas and human head models corresponding to both adults and children has been studied in detail. To this end, a semi-analytical technique has been developed to analyze the interaction between a layered spherical model of the human head and an arbitrarily shaped wire antenna radiating at its close proximity. The proposed technique is based on the combination of the Green's function methodology with the MoM. Extensive validation checks of the developed method have been performed and numerical results for homogeneous and three-layer head models corresponding to adults and children, exposed to the radiation of a helical dipole antenna at 1710 MHz have been presented. The developed method can be efficiently used for investigating the effect of various parameters on the power absorption by the head as well as on the antenna performance. Additionally, since the proposed technique is general as far as the wire antenna geometry is considered, it can provide an efficient and accurate tool for testing and comparison of different antenna designs. Finally, it can be employed as a reliable tool for benchmarking of purely numerical techniques. In this context, the accuracy of FDTD simulations has been checked against results produced by the Green/MoM technique and then FDTD has been used to solve the problem of a realistic handset equipped with a helix monopole antenna interacting with realistic head models based on MRI scans. Results produced have revealed that similar levels of absorbed power between adults and children head models are observed while also peak SAR values and power absorbed by the user's head are significantly lower for realistic exposure problems as compared to canonical ones.

Acknowledgment

The authors wish to thank Dr. G. Stamatakos and Mr. A. Karafotias for providing parts of the Green's function calculation numerical code used in this study.

References

[1] J. D. Krauss, *Antennas*, 2nd ed. New York: McGraw-Hill, 1988.

[2] K. S. Yee, "Numerical solution of initial boundary value problems involving Maxwell's equations in isotropic media," *IEEE Trans. Antennas Propagat.*, vol. 14, pp. 302–307, May 1966.

[3] T. S. C. Hagness, *Computational Electrodynamics: The Finite-Difference Time-Domain Method*, 2nd ed. Norwood, MA: Artech House, 2000.

[4] J. S. Colburn and Y. Rahmat-Samii, "Human proximity effects on circular polarized handset antennas in personal satellite communications," *IEEE Trans. Antennas Propagat.*, vol. 46, pp. 813–820, June 1998.

[5] J. T. Rowley, R. B. Waterhouse, and K. H. Joyner, "Modeling of normal-mode helical antennas at 900 GHz and 1.8 GHz for mobile communications handsets using the FDTD technique," *IEEE Trans. Antennas Propagat.*, vol. 50, pp. 812–819, June 2002.

[6] P. Bernardi, M. Cavagnaro, S. Pisa, and E. Piuzzi, "Power absorption and temperature elevations induced in the human head by a dual-band monopole-helix antenna phone," *IEEE Trans. Microwave Theory Tech.*, vol. 49, pp. 2539–2546, Dec. 2001.

[7] G. Lazzi and O. P. Gandhi, "On modeling and personal dosimetry of cellular telephone helical antennas with the FDTD code," *IEEE Trans. Antennas Propagat.*, vol. 46, pp. 525–530, Apr. 1998.

[8] G. Lazzi, Q. S. Yu, and O. P. Gandi, "Extension and validation of the equivalent sources helical antenna modeling with the FDTD code," in *Proc. IEEE Antennas and Propagation Society Int. Symp.*, vol. 2, July 1999, pp. 1054–1057.

[9] G. Cerri, S. Chiarandini, and P. Russo, "Numerical aspects in time domain modeling of arbitrarily curved thin wire antennas," *Int. J. Numer. Model.*, vol. 12, no. 4, pp. 275–294, 1999.

[10] M. A. Mangoud, R. A. Abd-Alhameed, and P. S. Excell, "Simulation of human interaction with mobile telephones using hybrid techniques over coupled domains," *IEEE Trans. Antennas Propagat.*, vol. 48, pp. 2014–2021, Nov. 2000.

[11] K. S. Nikita *et al.*, "A study of uncertainties in modeling antenna performance and power absorption in the head of a cellular phone user," *IEEE Trans. Microwave Theory Tech.*, vol. 49, pp. 2676–2687, Dec. 2000.

[12] P. M. Morse and H. Feshbach, *Methods of Theoretical Physics*. New York: Mc Graw-Hill, 1953, pt. II, ch. 13.

[13] P. Cottis and N. K. Uzunoglu, "Focusing properties of dipole arrays placed near a multilayer lossy sphere," *J. Electromagn. Waves Applicat.*, vol. 4, pp. 431–440, 1990.

[14] K. S. Nikita, G. S. Stamatakos, N. K. Uzunoglu, and A. Karafotias, "Analysis of the interaction between a layered spherical human head model and a finite-length dipole," *IEEE Trans. Microwave Theory Tech.*, vol. 48, pp. 2003–2013, Nov. 2000.

[15] D. J. Struik, *Lectures on Classical Differential Geometry*, 2nd ed. New York: Dover, 1961, ch. 1.

[16] R. F. Harrington, "Matrix methods for field problems," *Proc. IEEE*, vol. 55, pp. 136–149, Feb. 1967.

[17] FCC, "Additional information for evaluating compliance of mobile and portable devices with FCC limits for human exposure to radiofrequency emissions," FCC, Washington, DC, FCC OET BULLETIN 65—Suppl. C, 1997.

[18] CENELEC, "Considerations for human exposure to electromagnetic fields from mobile telecommunication equipment (MTE) in the frequency range 30 MHz –6 GHz," CENELEC, Brussels, Belgium, CENELEC, prES 59 005, 1997.

[19] "Guidelines for limiting exposure to time-varying electric, magnetic and electromagnetic fields (up 300 Ghz)," *Health Phys.*, vol. 56, 1998.

[20] *IEEE Standard for Safety Levels With Respect to Human Exposure to Radio-Frequency Electromagnetic Fields, 3 kHz–300 GHz*, IEEE Standard C9.51, 1999.

[21] EC, "Council recommendation for the limitation of exposure of the general public to electromagnetic fields (0 Hz to 300 GHz)," EC, 1999/519/EC, 1999.

[22] "Electromanetic Solver Based on the Finite Difference Time Domain Method," Remcom Inc.

[23] J. P. Berenger, "A perfectly matched layer for the absorption of electromagnetic waves," *J. Comput. Phys.*, vol. 4, pp. 185–200, 1994.

[24] S. Gabriel and E. Corthout, "The dielectric properties of biological tissues," *Med. Phys.*, vol. 41, pp. 2231–2293, 1996.

[25] P. Olley and P. S. Excell, "Classification of a high-resolution voxel image of a human head," in *Proc. Int. Workshop at the National Radiological Protection Board*, P. J. Dimbylow, Ed., Chilton, U.K., 1995, pp. 16–23.

[26] H. Durney, H. Massoudi, and M. F. Iskander, *Radiofrequency Radiation Dosimetry Handbook*, 4th ed. Brooks Air Force Base, TX: USAF School of Aerospace Medicine, Aerospace Med. Div, (AFSC), , 1986.

[27] S. Koulouridis and K. S. Nikita, "Characteristics of power absorption in human head models exposed to normal-mode helical antennas," in *Proc. 2nd Int. Workshop Biological Effects of EMF*, Rhodes, Greece, Oct. 2002, pp. 241–250.

Stavros Koulouridis was born in Athens, Greece, in 1975. He received the Diploma and the Ph.D. degrees in electrical and computer engineering from the National Technical University of Athens (NTUA), Athens, Greece, in 1999 and 2003, respectively.

His research interests include computational electromagnetism, microwave applications in medicine, parallel processing applications in electromagnetism. He has authored 11 papers in international conferences and journals. He teaches in the "School of Pedagogic and Technological Education (ASPAITE)," since 2000.

Konstantina S. Nikita (M'96-SM'00) received the Diploma in electrical engineering and the Ph.D. degree from the National Technical University of Athens (NTUA), Athens, Greece, in 1986 and 1990, respectively, and the M.D. degree from the University of Athens, Athens, Greece, in 1993.

Since 1990, she has been working as a Researcher at the Institute of Communication and Computer Systems, National Technical University of Athens. In 1996, she joined the Department of Electrical and Computer Engineering, NTUA, where she is currently an Associate Professor. Her current research interests include computational bioelectromagnetics, applications of electromagnetic waves in medicine, medical imaging and image processing, biomedical informatics, health telematics, simulation of physiological systems. She has authored or coauthored 80 papers in refereed international journals and chapters in books, and more than 150 papers in international conference proceedings. She holds one patent. She has been the Technical Manager of several European and National Research and Development projects in the field of biomedical engineering.

Dr. Nikita was the recipient of the 2003 Bodossakis Foundation Scientific Prize. She is a member of the Technical Chamber of Greece, the Athens Medical Association, and the Hellenic Society of Biomedical Engineering.